Non-Coherent FSK: An Attractive Modulation Set for Millimeter-Wave Communications

Ali A. Nasir*, Hani Mehrpouyan¶, David Matolak‡, and Salman Durrani§
*School of Electrical Engineering and Computer Science, National University of Sciences and Technology, Islamabad, Pakistan.
¶Department of Electrical and Computer Engineering and Computer Science, California State University, USA
‡College of Engineering and Computing, University of South Carolina, USA
Emails: ali.nasir@seecs.edu.pk, hani.mehr@ieee.org, matolak@cec.sc.edu, salman.durrani@anu.edu.au

***Abstract*—Millimeter-wave (mm-wave) systems suffer from an assortment of propagation and hardware challenges such as extremely high pathloss/shadowing and amplifier non-linearity/phase noise, respectively. In this paper, we demonstrate via simulations that non-coherent frequency shift keying (FSK) can utilize the vast bandwidth at mm-wave frequencies to combat significant pathloss and shadowing in this band, while being robust to amplifier non-linearity and phase noise. To support our findings, we establish a comprehensive simulation setup and set of parameters that consider the impact of pathloss, shadowing, amplifier non-linearity, and phase noise, at mm-wave frequencies. Our results indicate that non-coherent FSK outperforms other modulation schemes such as phase shift keying and quadrature amplitude modulation. This outcome combined with the low detection complexity of non-coherent FSK make it an attractive modulation for achieving multi Gbps wireless links at mm-wave frequencies. The proposed comprehensive simulation setup can also be applied to investigate and validate the performance of various mm-wave systems in practical settings.**

I. Introduction

It is anticipated that 5G cellular networks will support a significantly larger set of applications compared to 4G. These applications span sensor networks, the smart grid, the medical field, and vehicular communications [1]. Moreover, it is expected that 50 billion wireless devices will be deployed by 2020 [1]. A large portion of these devices will support machine-to-machine communications, e.g., autonomous vehicles. Hence, next generation cellular networks have to support a significantly larger number of users. To meet this demand on higher data capacity and higher data rates, 5G networks must take advantage of the frequencies in the millimeter-wave (mm-wave) band, i.e., 30–300 GHz [1], [2].

Given large bandwidth that is available for communications in the mm-wave band, the potential of mm-wave for establishing high speed communication links is well-understood. However, there are significant hurdles that need to be overcome before mm-wave communication systems can become mainstream. Some of these issues are related to the high free-space pathloss and shadowing that is present at mm-wave frequencies [2], [3]. In fact, for the same transmit power and data rate, mm-wave communication systems are expected to be able to support significantly shorter links when compared to wireless systems in the microwave band [4], [5]. Moreover, mm-wave systems are affected by other impairments such as amplifier non-linearity and phase noise that stem from the extremely high frequencies that the RF transceivers need to operate at [4], [6]. Thus, significant efforts are being made to address these issues through the use of massive multi-input multi-output systems (MIMO) [7], sophisticated relaying approaches [8], physical layer designs that are robust to amplifier non-linearity [9], and estimation and synchronization algorithms that mitigate the impact of phase noise [10], [11].

Although the above approaches are extremely effective at overcoming the aforementioned challenges at the mm-wave band, they add further complexity to the transceiver structures, which are already prohibitively high due to utilization of a very large bandwidth. The authors believe that simple solutions that can overcome the propagation and hardware impairments issues at this band may be better suited to utilize the vast bandwidth at mm-wave frequencies. As such, here, we focus on utilizing non-coherent frequency shift keying (FSK) for circumventing the challenges at mm-wave frequencies.

Rationale for proposing use of FSK: Due to the scarcity of bandwidth in the microwave band, non-coherent FSK has been mainly pushed to the sidelines in today's cellular networks. The M-ary non-coherent FSK utilizes a larger bandwidth as the size of the constellation, M, increases [12]. For example, a system utilizing 4 quadrature amplitude modulation (QAM) and achieving a data rate of 2 Gbps, requires 1 GHz of bandwidth. On the other hand, it can be easily calculated that a system using 4-ary non-coherent FSK and achieving the same data rate as above needs 4 times as much bandwidth or 4 GHz to be exact. However, unlike QAM or phase shift keying (PSK), where as the order of modulation set, M, increases the bit error rate (BER) of the system also increases, the BER of M-ary non-coherent FSK decreases with an increasing M [12]. Thus, M-FSK can use the large bandwidth at mm-wave frequencies* to achieve multi Gbps wireless links, while also improving the BER performance of the system. The latter can help overcome the issues associated with pathloss and shadowing in this band. In other words, we are indicating that it is beneficial to sacrifice bandwidth efficiency to achieve higher data rates and better BER performance using M-FSK since there is such an abundance of untapped bandwidth that

The work is in part supported by Department of Defense Grant, number W911NF-15-1-0033. The work of S. Durrani was supported by the Australian Research Council's Discovery Project Funding Scheme (project number DP140101133).

*From 57–64 GHz, 71–76 GHz, and 81–86 GHz. Moreover, there is even more bandwidth available that is still unlicensed including 120–180 GHz and 200–300 GHz.

is available at mm-wave frequencies.

The remainder of this paper also shows that M-FSK has other desirable properties that make it even more suitable for mm-wave applications. In fact, via extensive simulations we show that M-FSK is extremely robust to both phase noise and amplifier non-linearity. However, a survey of literature shows that non-coherent FSK has been mainly overlooked for applications in this band. Application of M-FSK in the mm-wave band has been briefly discussed in [6]. However, there are no discussions on the impact of phase noise and amplifier non-linearity on the performance of M-FSK. In [13], the authors briefly demonstrate the potential of FSK achieving high data rates in indoor environment at the mm-wave frequencies. However, again there are no investigations related to the effect of hardware impairments on the performance of M-FSK. The phase noise parameters for system using M-FSK has been analyzed in [14]. However, there are no performance evaluation on the actual effect of phase noise on the BER performance of M-FSK.

In this paper, we demonstrate via simulations that non-coherent FSK can utilize the vast bandwidth at mm-wave frequencies to combat significant pathloss and shadowing in this band, while being robust to amplifier non-linearity and phase noise. To support our findings, we establish a comprehensive simulation setup and set of parameters that consider the impact of pathloss, shadowing, amplifier non-linearity, and phase noise, at the 60 GHz band. Our results indicate that non-coherent FSK outperforms phase shift keying, and quadrature amplitude modulation, at mm-wave frequencies. This outcome combined with the low detection complexity of non-coherent FSK make it an attractive modulation for achieving multi Gbps wireless links at mm-wave frequencies. Moreover, the proposed comprehensive simulation setup can be applied to investigate and validate the performance of various mm-wave systems in practical settings.

This paper is organized as follows: in Section II the system model for the proposed mm-wave system is presented. Section III presents an extensive simulation setup for mm-wave systems that considers pathloss, shadowing, amplifier non-linearity, and phase noise, at the 60 GHz band. Section IV investigates the impact of these impairments on the performance of M-FSK, M-PSK, and M-QAM through extensive simulations. Finally, Section V concludes the paper.

II. System Model

Suppose an information symbol $x_n \in \mathbb{C}$ is transmitted over a wireless narrowband channel $h \in \mathbb{C}$ with additive noise $\nu_n \in \mathbb{C}$, where n is the symbol index. In practice, physical radio-frequency (RF) transceivers suffer from hardware impairments such as phase noise, amplifier non-linearity, and IQ imbalance. The combined influence of these impairments can be modeled by a generalized channel model [8], [10], where the received signal is

$$y_n = e^{j\phi_n} h(x_n + \eta) + \nu_n, \tag{1}$$

where ϕ_n corresponds to the nth sample of the phase noise and η is used to model the distortion noise that appear from the transceiver impairments, such as amplifier non-linearity and in-phase and quadrature-phase (IQ) imbalance [15]. Additive noise ν_n is assumed to be white and complex Gaussian process with $\nu_n \sim \mathcal{CN}(0, N_o)$, $\forall\ n$, and N_o is the noise power per unit bandwidth. Based on [16], [17], the phase noise process can be modeled as a Brownian motion or Wiener process and is given by

$$\phi_n = \phi_{n-1} + \Delta_n \tag{2}$$

where the phase noise innovation Δ_n is assumed to be white real Gaussian process with $\Delta_n \sim \mathcal{N}(0, \sigma^2_{\text{phn}})$ and σ^2_{phn} is variance of the phase noise innovation process [10]. The distortion noise due to hardware impairments η, in (1), can be modeled as a complex Gaussian process with $\eta \sim \mathcal{CN}(0, \sigma^2_{\text{nl}} P)$, where $P = \mathbb{E}_{x_n}\{|x_n|^2\}$ is the average power of the information symbols and σ^2_{nl} is the hardware distortion noise variance [15].

In (1), we model the wireless channel h by [2]

$$h = \sqrt{\frac{K(f_c)}{\psi}\left(\frac{d_o}{d}\right)^{\gamma}}\left(\sqrt{\frac{K_R}{1+K_R}}h_{\text{LOS}} + \sqrt{\frac{1}{1+K_R}}h_{\text{NLOS}}\right), \tag{3}$$

where

- $K(f_c) \triangleq \left(\frac{\lambda}{4\pi d_o}\right)^2$, $\lambda = \frac{c}{f_c}$ is the wavelength of the carrier signal, c is the speed of light, f_c is the carrier frequency, d_o is the reference distance,
- ψ is log-normally distributed random variable which models the shadowing effect, such that μ_{shad} and σ_{shad} are the mean and standard deviation of the corresponding normally distributed random variable $10\log_{10}\psi$,
- d is the distance between the transmitter and the receiver, γ is the path loss exponent,
- $h_{\text{LOS}} \triangleq e^{\frac{j2\pi a \sin\theta}{\lambda}}$ is the line-of-sight channel component, $a = \frac{\lambda}{2}$ is the antenna spacing, θ is the angle of arrival, $h_{\text{NLOS}} \sim \mathcal{CN}(0,1)$ is the complex normally distributed non-line of sight channel component, and the contribution of h_{LOS} and h_{NLOS} to the overall channel is denoted by the Rician factor K_R.

In (3), the factors $K(f_c)$, γ, and d correspond to the large scale fading while the factor $\sqrt{\frac{K_R}{1+K_R}}h_{\text{LOS}} + \sqrt{\frac{1}{1+K_R}}h_{\text{NLOS}}$ corresponds to the small scale fading in the wireless channel. Note that the model in (3) seems similar to the one used for microwave communication system, however mm-wave communication systems experience high levels of phase noise, amplifier non-linearity, shadowing, and pathloss [2]. The range of practical values for mm-wave systems are detailed in Table I.

We propose to use *non-coherent frequency shift keying (FSK)* modulation where the phase of two different information symbols from the modulation set is not necessarily be same and the signal is not continuous at bit transitions. The block diagrams for non-coherent FSK modulator and demodulator are given in [12]. Particularly, for orthogonality, the two frequencies from the modulation set must be integer multiple of $\frac{1}{2T_s}$ and their separation must be integer multiple of $\frac{1}{T_s}$, where T_s defines the symbol period. Though the bandwidth requirement for non-coherent FSK is large compared to

TABLE I
RANGE OF VALUES USED FOR DIFFERENT SIMULATION PARAMETERS [2], [8], [18], [19].

Simulation Parameters	Values
phase noise variance σ^2_{phn}	$\{10^{-4}, 10^{-3}, 10^{-2}, 10^{-1}\}$
hardware distortion noise variance σ^2_{nl}	$\{0.1, 0.2, 0.3\}$
shadowing-standard deviation σ_{shad}	$\{6, 7, \ldots, 12\}$ dB
pathloss exponent γ	$\{3, 3.5, \ldots, 5\}$

other modulation schemes, such as phase shift keying (PSK) and quadrature amplitude modulation (QAM), however, we are targeting mm-wave communication where bandwidth is plentiful and is less of a concern. The main advantage of non-coherent FSK is its low detection complexity and as demonstrated in the following section through simulations, it can utilize the vast bandwidth at mm-wave frequencies to combat significant pathloss and shadowing in this band, while at the same time being robust to amplifier non-linearity and phase noise.

III. SIMULATION SETUP FOR MM-WAVE SYSTEMS

In this section, we present a simulation setup for mm-wave systems that considers pathloss, shadowing, amplifier non-linearity, and phase noise. The simulation setup described below can be applied to investigate and validate the performance of various mm-wave systems in practical settings. The range of values considered for the simulation parameters in our paper is given in Table I where the details with references is given below. Note that we consider broader range of values to also test the performance of non-coherent FSK over worst-case hardware impairment and channel distortion.

Phase Noise: The effect of phase noise is more profound at high frequencies in mm-wave communication [3]. For the Si CMOS technology, it has been established in [18] that phase noise variance is $\sigma^2_{\text{phn}} = 10^{-3}$ rad^2 at $f_c = 60$ GHz and system bandwidth $= 1$ MHz.[†] Further, the phase noise variance increases by increasing the carrier frequency. In our simulation results, we investigate the effect of a range of phase noise variances $\sigma^2_{\text{phn}} = \{10^{-4}, 10^{-3}, 10^{-2}, 10^{-1}\}$ on the system performance.

Amplifier non-linearity: The effect of hardware impairment, e.g., amplifier nonlinearity is more severe at high frequencies in mm-wave communication [3]. Particularly, hardware distortion noise variance of $\sigma^2_{\text{nl}} = 0.15$ is considered to be extremely high for microwave communication [8]. There is presently no amplifier non-linearity model, as the one presented in [8], for mm-wave systems. Hence, we investigate the effect of range of distortion noise variances $\sigma^2_{\text{nl}} = \{0.1, 0.2, 0.3\}$ on the performance of different modulation schemes.

Shadowing: Empirical results and experiments, conducted for mm-wave communication systems in [20], establish that shadowing-standard deviation is $\sigma_{\text{shad}} = 9.13$ dB at 28 GHz. Considering the fact that we study the effect of channel distortions over a wide range of mm-wave frequencies 50-130 GHz, particularly over 60 GHz band, we consider the range of values of $\sigma_{\text{shad}} = \{6, 7, \ldots, 12\}$ dB to study the effect of shadowing on different modulation schemes.

Pathloss: The effect of pathloss is more significant at high frequencies in mm-wave communication due to atmospheric absorption [2]. It has been found through empirical results and experiments, conducted for mm-wave communication systems, that a signal transmitted from a 7 meter antenna height suffers from a path loss exponent of $\gamma = 3.73$ at 28 GHz [19]. In our results, we consider a range of values of path loss exponent, i.e,. $\gamma = \{3, 3.5, \ldots, 5\}$ to study its effect on different modulation schemes.

IV. SIMULATIONS RESULTS

In this section, the effect of hardware impairments and channel distortion on the performance of non-coherent FSK and different other modulation schemes, e.g., PSK and QAM, is studied through simulations. Particularly, we consider different modulation sizes, e.g., $M = \{4, 16, 64\}$ for non-coherent FSK, PSK, and QAM. To model small scale fading, we set the Rician factor $K_R = 5$ dB and the angle of arrival θ is a random number, i.e., uniformly distributed between 0 and 2π. To model large scale fading, we set the reference distance $d_o = 1$ meter and the distance between the transmitter and the receiver is set to $d = 25$ meters. Unless otherwise stated, we set the other large scale fading parameters, i.e., path loss exponent $\gamma = 4$ and carrier frequency $f_c = 60$ GHz. The average symbol power $P = \mathbb{E}_{x_n}\{|x_n|^2\}$ is set to 1 and the noise power density N_o is set relative to bit energy E_b, i.e, we set $\frac{E_b}{N_o} = 150$ dB at the transmitter, unless stated otherwise. *Note that* $\gamma 10\log_{10}\frac{d}{d_o} - 10\log_{10} K(f_c) = 124$ *dB 'loss' is straightforwardly caused by the transmission at carrier frequency* $f_c = 60$ *GHz and with path loss exponent* $\gamma = 4$ *and* $d = 25$ *meters. Thus,* $\frac{E_b}{N_o} = 150$ *dB at the transmitter translates to the value of* 26 *dB at the receiver if the signal attenuation due to carrier frequency* f_c *and path loss exponent* γ *is ignored, as usually assumed in many papers.* It is further noteworthy that $\frac{E_b}{N_o} = 150$ dB is a practical value since typical base station transmits at a power of 46 dBm and typical noise density is -174 dBm/Hz. All results are averaged over 10^5 simulations with each simulation performed over a frame length of 100 symbols. The individual effect of phase noise, hardware distortion noise (due to IQ imbalance and amplifier non-linearity), shadowing, path loss exponent, and carrier frequency, over the range of values of these parameters, on the system performance is studied in the following sections

[†]Note that for constant bit rate of say 2 Mbps, the bandwidth required by non-coherent M-FSK will be M MHz and that required by M-PSK or M-QAM will be 1 MHz.

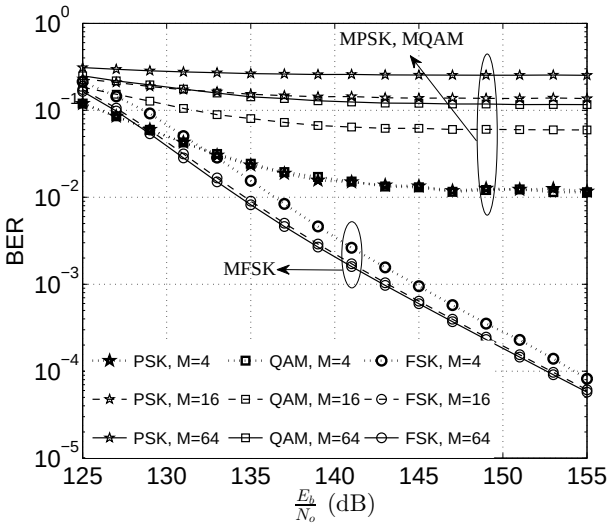

Fig. 1. BER versus $\frac{E_b}{N_o}$ at the transmitter (reflects to $\frac{E_b}{N_o} = \{1, 6, \ldots, 31\}$ dB at the receiver) with phase noise variance $\sigma^2_{\text{phn}} = 10^{-3}$.

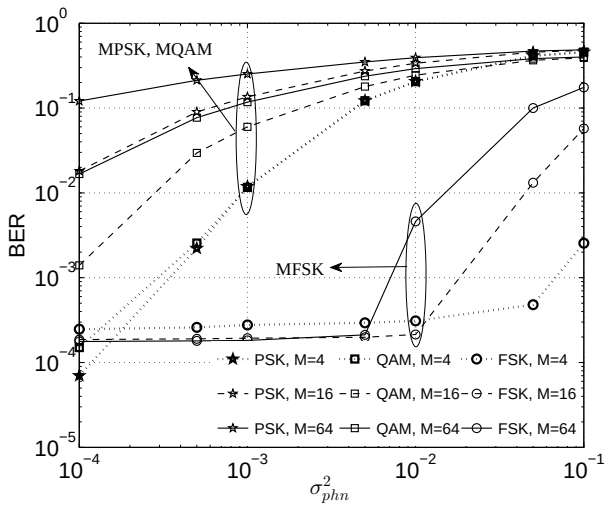

Fig. 2. BER versus phase noise variance σ^2_{phn} at $\frac{E_b}{N_o} = 150$ dB at the transmitter (reflects to $\frac{E_b}{N_o} = 26$ dB at the receiver).

(cf. Secs. IV-A-IV-C). Finally, the combined effect of all the hardware impairments and channel distortions will be studied in Sec. IV-D.

A. Effect of Phase Noise

Fig. 1 plots the bit-error rate (BER) versus $\frac{E_b}{N_o}$ for a fixed value of phase noise variance $\sigma^2_{\text{phn}} = 10^{-3}$ rad^2, while the effect of range of values of phase noise variance will be studied in Fig. 2. In Fig. 1, the range of values of $\frac{E_b}{N_o}$ in abscissa is between 125 and 155 dB. Again, note that if the signal attenuation of 124 dB caused by the transmission at carrier frequency $f_c = 60$ GHz and with path loss exponent $\gamma = 4$ and $d = 25$ meters, is ignored, $\frac{E_b}{N_o} = \{125, 130, \ldots, 155\}$ dB at the transmitter will translate to the range $\{1, \ldots, 31\}$ dB at the receiver, which is usually considered in many papers.

It can be observed from Fig. 1 that the application of M-PSK and M-QAM fails to achieve the BER of less than 10^{-2}, even at $\frac{E_b}{N_o} = 155$ dB. As a matter of fact, the BER of a system employing M-PSK and M-QAM suffers from an error floor and the level of the error floor increases by increasing the modulation order M due to denser constellations. On the other hand, the application of M-FSK achieves a BER $< 1 \times 10^{-4}$ at $\frac{E_b}{N_o} = 155$ dB. In addition, the BER of a system employing M-FSK decreases by increasing the modulation order M at the cost of increased bandwidth. However, we are targeting mm-wave communication where bandwidth is plentiful and is less of a concern. Even if we assume modulation size of $M = 4$, for which 4-FSK requires only 4 times more bandwidth compared to that required by 4-PSK or 4-QAM, BER for 4-FSK is 100 times smaller than that for 4-PSK or 4-QAM at $\frac{E_b}{N_o} = 155$ dB. On the other hand, if we use $M = 64$ (taking advantage of the ample bandwidth in mm-wave band), 64-FSK not only achieves more than 200 times smaller BER but also delivers 4 times higher throughput (bits per second) when compared to 4-PSK or 4-QAM. It is important to mention that in the absence of phase noise, the effect of the modulation order M on the BER performance of M-PSK, M-QAM, and M-FSK follows the similar trend (increasing the modulation order M increases the BER for M-PSK and M-QAM and decreases the BER for M-FSK [12, page 522]) as the one that we have observed in the presence of phase noise $\sigma^2_{\text{phn}} = 10^{-3}$.

In Fig. 2, we study the effect of range of values of phase noise variance on the BER performance at fixed value of $\frac{E_b}{N_o} = 150$ dB. It can be observed from Fig. 2 that M-FSK is capable of withstanding even severer phase noise, e.g., $\sigma^2_{\text{phn}} = 10^{-2}$ rad^2, where the application of M-PSK and M-QAM completely fails to help decode the received signal (BER $> 3 \times 10^{-1}$). Moreover, in case if phase noise gets extremely worse due to poor oscillators, e.g., $\sigma^2_{\text{phn}} = 10^{-1}$ rad^2, employing 4-FSK can still achieve the BER $= 2.4 \times 10^{-3}$ where all other modulation schemes fails to recover the transmitted information. An important engineering insight is that the usual trend of M-FSK, i.e., increasing the modulation order M decreases the BER, is observed in the opposite way for strong values of phase noise variance $\sigma^2_{\text{phn}} \geq 10^{-2}$ rad^2.

B. Effect of Other Hardware Distortions

In this subsection, we study the effect of other hardware distortions, such as amplifier non-linearity and IQ imbalance, modeled by η in (1), on the performance of different modulation schemes. Fig. 3 plots the bit-error rate (BER) versus $\frac{E_b}{N_o}$ for a fixed value of hardware distortion noise variance $\sigma^2_{\text{nl}} = 0.2$, while the effect of range of values of distortion noise variance will be studied shortly in Fig. 4. Similar to the case of phase noise as observed in Fig. 1, it can be observed from Fig. 3 that the presence of hardware impairments has a very destructive effect on the application of M-PSK and M-QAM, i.e., the BER suffers from an error floor and is greater than 10^{-2} even at $\frac{E_b}{N_o} = 155$ dB. On the other hand, employing M-FSK achieves the BER $< 1.3 \times 10^{-4}$ at $\frac{E_b}{N_o} = 155$ dB. As expected, increasing the modulation size from $M = 4$ to $M = 16$ or 64 decreases the BER of M-FSK-based system.

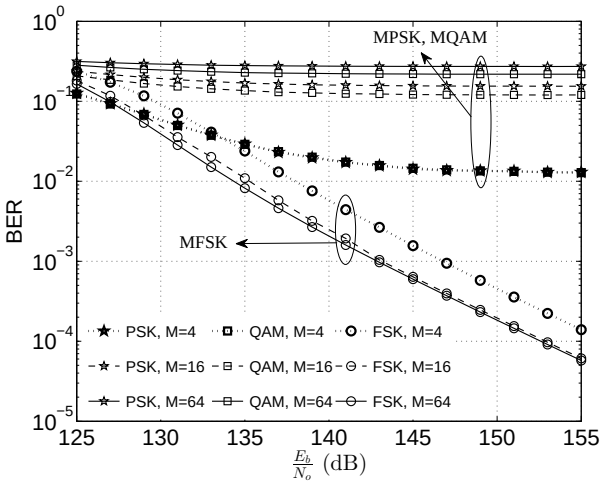

Fig. 3. BER versus $\frac{E_b}{N_o}$ at the transmitter (reflects to $\frac{E_b}{N_o} = \{1, 6, \ldots, 31\}$ dB at the receiver) with hardware distortion noise variance $\sigma^2_{\text{nl}} = 0.2$.

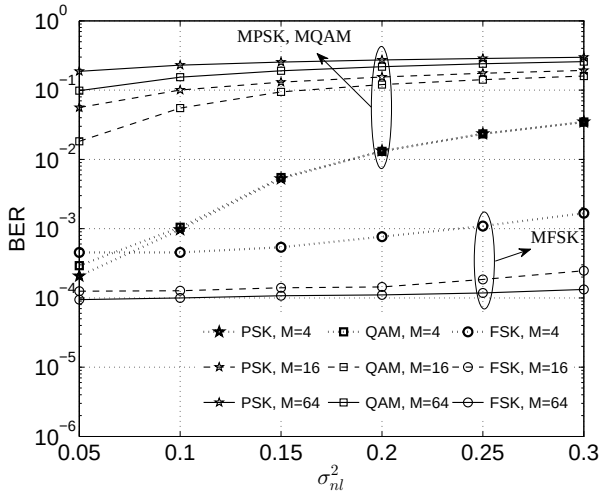

Fig. 4. BER versus hardware distortion noise variance σ^2_{nl} at $\frac{E_b}{N_o} = 150$ dB at the transmitter (reflects to $\frac{E_b}{N_o} = 26$ dB at the receiver).

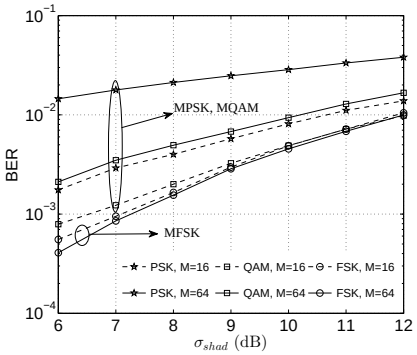

(a) shadowing standard deviation σ_{shad}

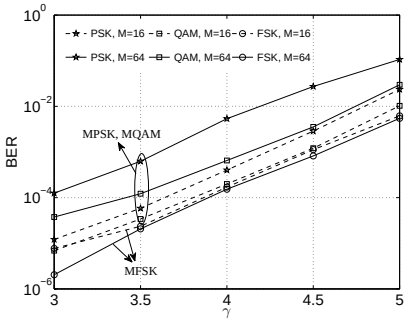

(b) path loss exponent γ

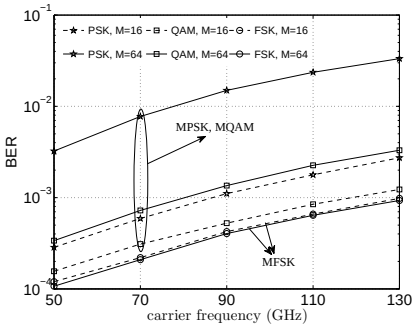

(c) carrier frequency f_c

Fig. 5. BER versus (a) shadowing standard deviation σ_{shad}, (b) path loss exponent γ, and carrier frequency f_c, at $\frac{E_b}{N_o} = 150$ dB at the transmitter (reflects to $\frac{E_b}{N_o} = 26$ dB at the receiver).

Though, this is at the expense of increased bandwidth, but that does not matter much for mm-wave communication. It is noteworthy that for modulation size $M = 4$ and 64, BER for MFSK is about 100 and 3000 times, respectively, smaller than that for PSK or QAM at $\frac{E_b}{N_o} = 155$ dB.

In Fig. 4, we study the effect of range of values of hardware distortion noise variance on the BER performance at fixed value of $\frac{E_b}{N_o} = 150$ dB. It can be observed from Fig. 2 that BER for M-FSK is smaller than 2×10^{-3} even against very strong effect of hardware impairment, e.g., $\sigma^2_{\text{nl}} = 0.3$, where the application of M-PSK and M-QAM may fail to recover the transmitted signal due to corresponding very high BERs. It is important to mention that BER performance for 64-FSK almost remains unaffected for the range of values of hardware distortion noise variance $\sigma^2_{\text{nl}} = (0.05, 0.3)$.

C. Effect of Large Scale Channel Fading

In this subsection, we will study the effect of large scale fading parameters, such as shadowing, path loss exponent, and carrier frequency, on the performance of different modulation schemes. Fig. 5 plots the BER versus shadowing-standard deviation σ_{shad} (Fig. 5(a)), (b) path loss exponent γ (Fig. 5(b)), and carrier frequency f_c (Fig. 5(c)), at $\frac{E_b}{N_o} = 150$ dB at the transmitter (which corresponds to 26 dB at the receiver). For clarity, the results are plotted only for modulation sizes $M = \{16, 64\}$. As expected, the BER performance for all modulation schemes gets worse by increasing shadowing-standard deviation σ_{shad}, path loss exponent γ, and carrier frequency f_c.

Fig. 5(a) displays the effect of shadowing on the system BER performance. We consider the range of values of $\sigma_{\text{shad}} = \{6, 7, \ldots, 12\}$ dB to study the effect of shadowing on different modulation schemes. Fig. 5(a) shows that M-FSK offers smaller BER compared to M-PSK and M-QAM for the whole set of considered values of shadowing-standard deviation σ_{shad}. Particularly, for $\sigma_{\text{shad}} = 9$ dB, 16-FSK achieves the BER $= 3 \times 10^{-3}$ which is 1.57 and 1.1 times smaller than that achieved by 16-PSK and 16-QAM, respectively. Similarly, 64-FSK achieves the BER $= 3 \times 10^{-3}$ which is 8.5 and 2.3 times smaller than that achieved by 64-PSK and 64-QAM,

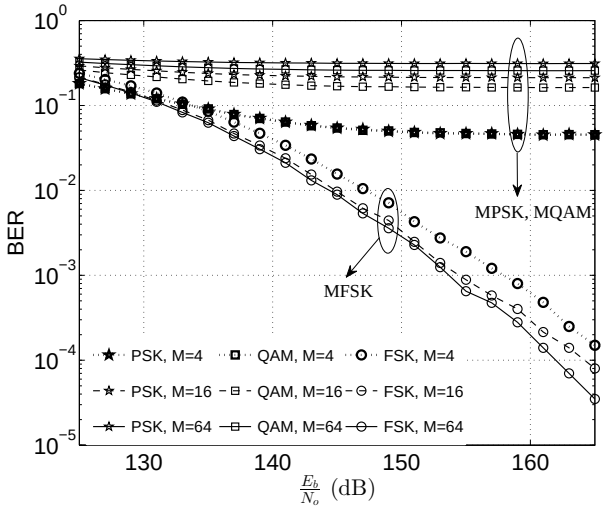

Fig. 6. BER versus $\frac{E_b}{N_o}$ at the transmitter (reflects to $\frac{E_b}{N_o} = \{1, 6, \ldots, 41\}$ dB at the receiver) with all channel distortion and hardware impairments, e.g., phase noise variance $\sigma^2_{\text{phn}} = 10^{-3}$, hardware distortion noise variance $\sigma^2_{\text{nl}} = 0.2$, shadowing-standard deviation $\sigma^2_{\text{shad}} = 9$ dB, path loss exponent $\gamma = 4$, and carrier frequency $f_c = 60$GHz.

respectively.

Fig. 5(b) plots the effect of varying path loss exponent on the system BER performance. We consider the range of values of path loss exponent, i.e,. $\gamma = \{3, 3.5, \ldots, 5\}$ to study its effect on different modulation schemes. Fig. 5(b) shows that M-FSK offers smaller BER compared to M-PSK and M-QAM for the whole set of considered values of path loss exponent γ. Particularly, for $\gamma = 4$ dB, 16-FSK achieves the BER $= 1.7 \times 10^{-4}$ which is 2.3 and 1.2 times smaller than that achieved by 16-PSK and 16-QAM, respectively. Similarly, 64-FSK achieves the BER $= 1.5 \times 10^{-4}$ which is 35.3 and 4.3 times smaller than that achieved by 64-PSK and 64-QAM, respectively.

Fig. 5(c) shows the BER performance for different modulation schemes and carrier frequencies. We know that mm-wave band can operate in the frequency range of $(30, 300)$ GHz. In Fig. 5(c), we plot the results for the carrier frequency range $f_c = \{50, 70, \ldots, 110\}$ GHz. Note that we assume same value of path loss exponent $\gamma = 4$ in Fig. 5(c), however, atmospheric absorption due to oxygen is substantial at 60 GHz, when compared to that at other frequencies. Since, we assume $d = 25$ meters, signal attenuation due to oxygen absorption at 60 GHz (25 dB/km) is only 0.5 dB. Thus, same value of path loss exponent $\gamma = 4$ is used to plot the results in Fig. 5(c). As expected, the BER increases by increasing the carrier frequency, which implies that in order to achieve the same BER at higher carrier frequencies, the supportable distance between transmitter and receiver decreases. Fig. 5(c) shows that M-FSK offers smaller BER compared to M-PSK and M-QAM for the whole set of considered values of carrier frequency f_c. Particularly, for $f_c = 90$ GHz, 16-FSK achieves the BER $= 4.2 \times 10^{-4}$ which is 2.61 and 1.23 times smaller than that achieved by 16-PSK and 16-QAM, respectively. Similarly, 64-FSK achieves the BER $= 4 \times 10^{-4}$ which is 37.5 and 3.2 times smaller than that achieved by 64-PSK and 64-QAM, respectively.

D. Combined Effect of Hardware Impairments and Channel Distortions

Finally, Fig. 6 plots the most important results where we take into account the effect of all hardware impairments and the channel distortions. Specifically, we set the phase noise variance $\sigma^2_{\text{phn}} = 10^{-3}$, hardware distortion noise variance $\sigma^2_{\text{nl}} = 0.2$, shadowing-standard deviation $\sigma^2_{\text{shad}} = 9$ dB, path loss exponent $\gamma = 4$, and carrier frequency $f_c = 60$GHz. Fig. 6 plots the BER for different modulation schemes against the range of values of $\frac{E_b}{N_o} = \{125, 130, \ldots, 165\}$ dB at the transmitter. *Again, note that if the signal attenuation of* 124 *dB caused by the transmission at carrier frequency* $f_c = 60$ *GHz and with path loss exponent* $\gamma = 4$ *(see calculations in Sec. IV), is ignored,* $\frac{E_b}{N_o} = \{125, 130, \ldots, 165\}$ *dB at the transmitter will translate to the range* $\{1, 6, \ldots, 41\}$ *dB at the receiver, which is the range usually assumed in many papers.* It can be observed from Fig. 6 that the combined effect of hardware impairments and channel distortions is very destructive on the application of M-PSK and M-QAM, i.e., the BER suffers from an error floor and is greater than 4×10^{-2} even at $\frac{E_b}{N_o} = 165$ dB. On the other hand, employing M-FSK achieves the BER $< 2 \times 10^{-3}$ at $\frac{E_b}{N_o} = 155$ dB. Specifically, by employing M-FSK, the BER does not suffer from an error floor under the considered wide range of $\frac{E_b}{N_o}$ and gets even lower than 2×10^{-4} at $\frac{E_b}{N_o} = 165$ dB. As expected, increasing the modulation size from $M = 4$ to $M = 16$ or 64 decreases the BER of M-FSK-based communication system. If we assume modulation size of $M = 4$, for which FSK requires only 4 times more bandwidth compared to that required by PSK or QAM, BER for FSK is about 315 times smaller than that for PSK or QAM at $\frac{E_b}{N_o} = 165$ dB. On the other hand, if we enjoy the ample bandwidth available for mm-wave communication, 64-FSK not only achieves more than 1300 times smaller BER but also delivers 4 times higher throughput (bits per second) when compared to 4-PSK or 4-QAM.

V. Conclusion

In this paper, we have demonstrated the application advantages of non-coherent FSK over other modulations schemes, e.g., PSK and QAM at 60 GHz band in the presence of hardware impairments and channel distortions. Through extensive system-level simulations, we have shown that non-coherent FSK, while enjoying vast bandwidth at mm-wave frequencies, combats the severe effect of pathloss, shadowing, amplifier non-linearity, and phase noise quite better than other modulations schemes such as PSK and QAM. For example,

- Considering the effect of hardware impairments (phase noise in Fig. 1 and amplifier non-linearity in Fig. 3) individually, our extensive simulations show that BER for 4-ary non-coherent FSK is about 100 times smaller as compared to the BER for 4-PSK or 4-QAM at transmitter $\frac{E_b}{N_o} = 155$ dB (receiver $\frac{E_b}{N_o} = 31$ dB). Similarly, considering the effect of channel distortions (shadowing in Fig. 5(a) and pathloss in Fig. 5(b)) individually, our extensive simulations show that BER for 16-ary non-coherent FSK is about 1.57 and 2.3 times, respectively,

smaller as compared to the BER for 16-PSK or 16-QAM at transmitter $\frac{E_b}{N_o} = 150$ dB (receiver $\frac{E_b}{N_o} = 26$ dB).

- Considering the effect of all hardware and channel impairments together (Fig. 6), our extensive simulations show that BER for 4-ary non-coherent FSK is about 315 times smaller as compared to the BER for 4-PSK or 4-QAM at transmitter $\frac{E_b}{N_o} = 165$ dB (receiver $\frac{E_b}{N_o} = 41$ dB).

This remarkable gain in terms of BER, combined with the low detection complexity of non-coherent FSK, makes it an attractive modulation for achieving multi Gbps wireless links at mm-wave frequencies. Since we have not considered coding or any receiver design to compensate the effect of hardware non-linearities, the performance comparison of different modulation schemes in their presence can be the subject of future research.

REFERENCES

[1] A. Osseiran *et al.*, "Scenarios for 5G mobile and wireless communications: The vision of the METIS project," vol. 52, no. 5, pp. 26–35, May 2014.

[2] T. S. Rappaport, R. W. Heath, R. C. Daniels, and N. Murdock, *Millimeter-Wave Wireless Communications*. Prentice Hall, 2014.

[3] H. Mehrpouyan, M. Khanzadi, M. Matthaiou, A. Sayeed, R. Schober, and Y. Hua, "Improving bandwidth efficiency in e-band communication systems," *IEEE Commun. Mag.*, vol. 52, no. 3, pp. 121–128, March 2014.

[4] J. Wells, *Multigigabit Microwave and Millimeter-Wave Wireless Communications*. Artech House, 2010.

[5] H. Mehrpouyan, M. Matthaiou, R. Wang, and G. K. Karagiannidis, "Hybrid millimeter-wave systems: A novel paradigm for HetNets," vol. 53, no. 1, pp. 216–221, Jan. 2014.

[6] K.-C. Huang and Z. Wang, *Millimeter Wave Communication Systems*. John Wiley & Sons, 2011.

[7] A. L. Swindlehurst, E. Ayanoglu, P. Heydari, and F. Capolino, "Millimeter-wave massive MIMO: The next wireless revolution?" vol. 52, no. 9, pp. 56–62, Sep. 2014.

[8] M. Matthaiou, A. Papadogiannis, E. Bjornson, and M. Debbah, "Two-way relaying under the presence of relay transceiver hardware impairments," *IEEE Commun. Lett.*, vol. 17, no. 6, pp. 1136–1139, Jun. 2013.

[9] S. Thompson *et al.*, "Constant envelope OFDM," vol. 56, no. 8, pp. 1300–1312, Aug. 2008.

[10] H. Mehrpouyan, A. Nasir, S. Blostein, T. Eriksson, G. Karagiannidis, and T. Svensson, "Joint estimation of channel and oscillator phase noise in MIMO systems," *IEEE Trans. Signal Processing*, vol. 60, no. 9, pp. 4790–4807, Sep. 2012.

[11] A. A. Nasir, H. Mehrpouyan, R. Schober, and Y. Hua, "Phase noise in MIMO systems: Bayesian Cramer-Rao bounds and soft-input estimation," *IEEE Trans. Signal Processing*, vol. 61, no. 10, pp. 2675–2692, May 2013.

[12] B. Sklar, *Digital Communciations*. Prentice Hall, 2001.

[13] C. S. Bontu, D. D. Falconer, and L. Strawczynski, "Feasibility evaluation of high rate FSK data transmission and equalization for millimeter wave indoor radio," in *Proc. IEEE Int. Conf. Universal Personal Commu.*, Dec 1996, pp. 822–826.

[14] J. Alexovich and R. Gagliardi, "The effect of phase noise on noncoherent digital communications," vol. 38, no. 9, pp. 1539–1548, Sep. 1990.

[15] D. K. Nguyen, M. Matthaiou, T. Q. Duong, and H. Ochi, "RF energy harvesting two-way cognitive DF relaying with transceiver impairments," in *Proc. IEEE ICC*, 2015.

[16] A. Demir, A. Mehrotra, and J. Roychowdhury, "Phase noise in oscillators: A unifying theory and numerical methods for characterization," *IEEE Trans. Circuits Syst.*, vol. 47, no. 5, p. 655674, May 2000.

[17] A. Chorti and M. Brookes, "A spectral model for RF oscillators with power law phase noise," *IEEE Trans. Circuits Syst.*, vol. 53, no. 9, pp. 1989–1999, Sep. 2006.

[18] M. Khanzadi, R. Krishnan, D. Kuylenstierna, and T. Eriksson, "Oscillator phase noise and small-scale channel fading in higher frequency bands," in *Proc. IEEE Globecom*, Dec 2014, pp. 410–415.

[19] G. R. MacCartney, J. Zhang, S. Nie, and T. S. Rappapor, "Path loss models for 5G millimeter wave propagation channels in urban microcells," in *Proc. IEEE Globecom*, 2013.

[20] S. Sun and T. Rappaport, "Wideband mmwave channels: Implications for design and implementation of adaptive beam antennas," in *Proc. IEEE IMS*, 2014.